Micro-Raman spectral analysis of the subsurface damage layer in machined silicon wafers

Long-Qing Chen, Xin Zhang, and Tong-Yi Zhang
Department of Mechanical Engineering, Hong Kong University of Science and Technology, Clear Water Bay, Kowloon, Hong Kong

H.Y. Lin and Sanboh Lee
Department of Materials Science, National Tsing Hua University, Hsinchu, Taiwan, Republic of China

(Received 25 October 1999; accepted 25 April 2000)

In the present work we studied the depth of damage layer in machined silicon wafers that was incorporated with chemical etching using micro-Raman spectroscopy. Subsurface damage causes changes in the shape and intensity for the shoulder (450–570 cm^{-1}) of the most intense band (519 cm^{-1}) and the second band (300 cm^{-1}) regions of the Raman spectrum. Etching reduces the thickness of the damage layer and, hence, the intensities at the shoulder and the second band. The intensities at the shoulder and the second band become stable when the damage layer is completely etched out. The shoulder consists of two Gaussian profiles: the major and the minor. The band for the major profile is independent of etching depth, but the band for the minor profile shifts toward the longer wave numbers with increasing etching period until the damage layer is completely etched out. The depth of the damage layer is determined by the profiles of the shoulder and the second band and confirmed by the band shift of the minor profile. Transmission electron microscopy (TEM) further verified the results with respect to the depth of the damage layer. TEM observation showed that dislocations and stacking faults are responsible for the subsurface damage.

Silicon is the basic material widely used in the semiconductor industry. More than 90% of semiconductor devices are made of silicon. Because of the trend toward using larger and larger silicon wafers in fabrication of microelectronic devices, new requirements in wafer machining and quality control have become increasingly important.[1,2] Silicon wafers are manufactured from silicon ingots through the machining process including inner diameter cut-off grinding, lapping, normal grinding, chemical etching, and polishing. The machining processing may induce surface and subsurface damage in the wafers.[3,4] The depth of damage layer is defined as the distance from the specimen surface to the layer below which the lattice remains perfect.[5] The damage layer consists of various defects such as dislocations, voids, precipitates, or/and microcracks, etc.[6] These defects deteriorate the physical and chemical properties of silicon wafers and may locally break the lattice symmetry.[7–10]

Various techniques are employed to characterize the surface and subsurface damage.[10–13] Raman spectroscopy (or inelastic scattering) is an important tool for the analysis of surface layer of silicon wafers. For example, Raman spectroscopy was used to identify the phase and composition and to determine the short-range and long-range order and impurity configurations.[14–16] The effect of crystal size leads to shift the excitation maximum to lower energies and to additional band broadening.[16] Residual stresses were also studied on the basis of the band shift of Raman spectra.[5,7,17,18] Subsurface damage may induce residual stresses and, thus, can be assessed by Raman spectroscopy on the basis of the band shift.[5,9,12]

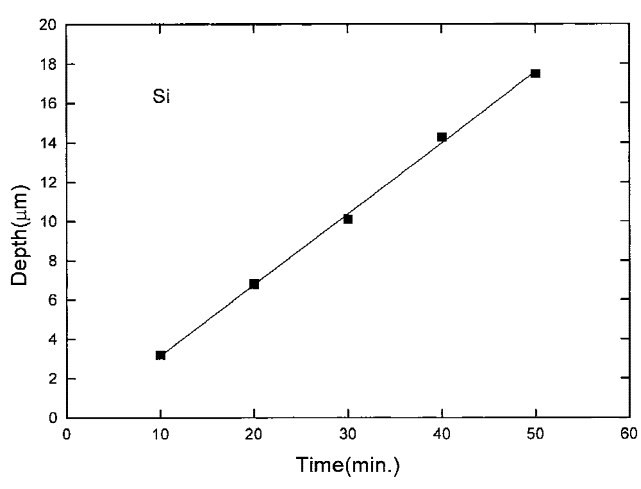

FIG. 1. Etching depth of silicon as a function of etching time at 60 °C.

In this paper, we use micro-Raman spectroscopy to estimate the depth of the damage layer in the machined silicon wafers.

Two kinds of polished silicon wafers (with 20- and 10-cm diameters) were provided by Mitsubishi Company, Tokyo, Japan, and Sino-American Silicon Products Inc., Hsinchu, Taiwan, respectively. All wafers were first annealed at 900 °C for 2 h and then machined with different conditions. Let S1, S2, S3, S4, and S5 denote wafers with the five different final processes of grinding (1200 mesh, 4000 mesh, 8000 mesh, grinding and polishing, and lapping, respectively). The wafer diameter is 20 cm for S2 and S3 and 10 cm for S1, S4, and S5. All specimens cut from the machined wafers have a size of 1 × 1 cm.

The chemical etching was carried out in a solution containing 40 wt% potassium hydroxide (KOH) inside a sealed container at 60 °C. A specimen was etched in KOH solution for 1, 3, 5, 10, 30, 60, 180, or 300 min. A shelter spot of low-temperature oxide (LTO) was designed and fabricated as a reference for measurement of the etching depth of the specimen. The step height between the LTO spot and the wafer surface before and after etching was measured, and their difference yields the etching depth. The Raman spectroscopy was conducted with a Renishaw model 3000 Micro-Raman/Photoluminescence System made by Renishaw, Gloucestershire, England, at room temperature. The argon ion laser beam of 514.5-nm wavelength with a power of 0.5 mW was focused onto a 2-μm spot on the specimen using an optical microscopy with a 50× objective lens. The wavelength was scanned in the range from 200 to 800 cm^{-1}.

Transmission electron microscopy (TEM) was conducted on a model JEM-2010 TEM system made by JEOL, Tokyo, Japan, with a working voltage 200 kV. Specimens were prepared by mechanical polishing to about 30 μm and then thinned by ion milling.

Figure 1 shows the etching depth as a function of etching time. The experimental data are well fitted with a straight line, and its slope yields the etching rate of 0.36 μm/min. Figures 2(a)–2(e) illustrate the Raman spectra for specimens S1, S2, S3, S4, and S5, respectively, with different etching times. It can be seen from Fig. 2 that intensities at the shoulder (450–570 cm^{-1}) for the most intense band (519 cm^{-1}) and the second band

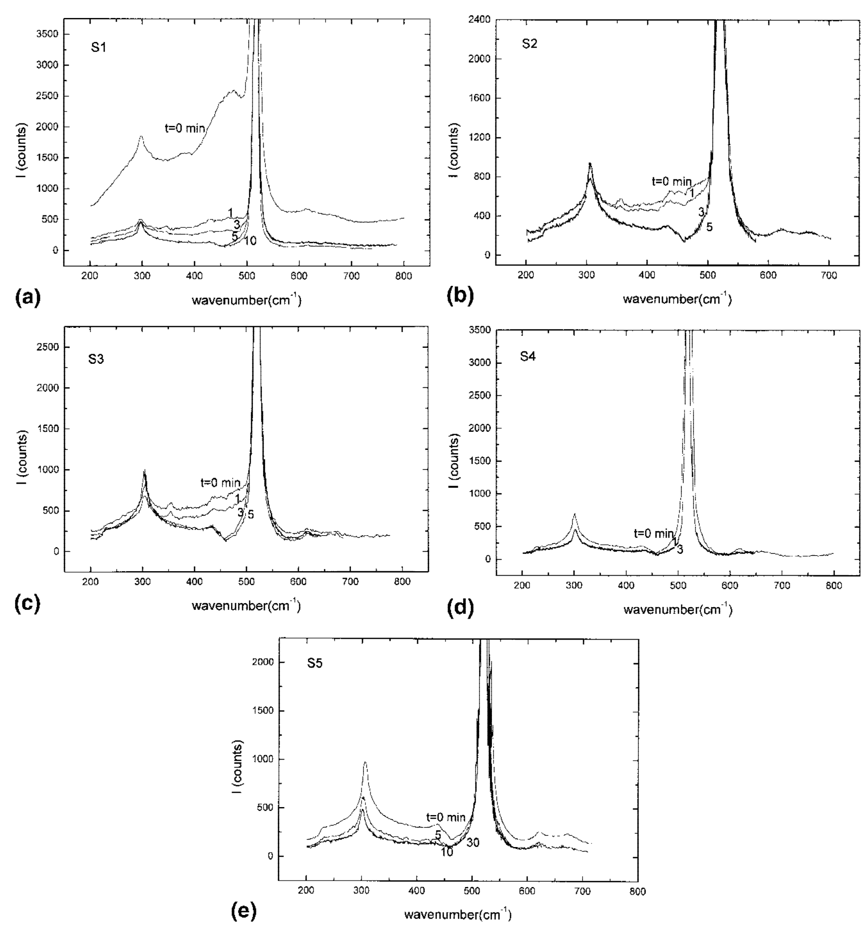

FIG. 2. Raman spectra for different specimens (a) S1, (b) S2, (c) S3, (d) S4, and (e) S5.

regions (450–570 cm^{-1}) decrease with increasing etching period until the profile becomes stable. The spectra become stable after 10, 3, 5, 1, and 10 min of etching for S1, S2, S3, S4, and S5, respectively. Thus, the depth of subsurface damage for S1, S2, S3, S4, and S5 are estimated to be about 3.6, 1.08, 1.80, 0.36, and 3.60 μm. The Raman spectrum at the shoulder for the most intense band consists of two overlapped features between 450 and 570 cm^{-1}. The Raman spectra in this range can be fitted by the sum of two Gaussian profiles as

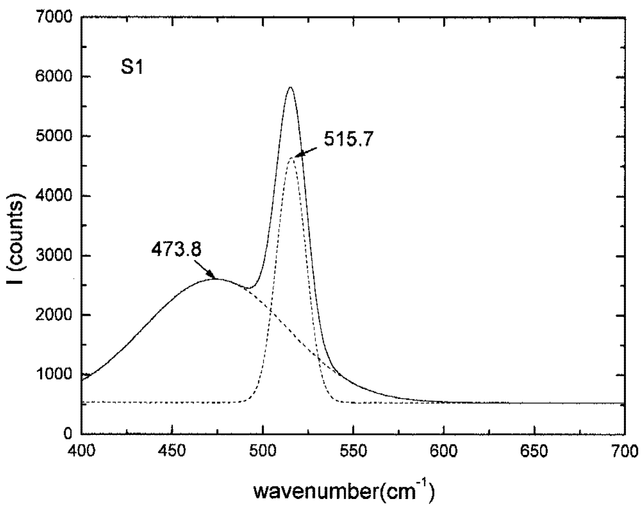

FIG. 3. Solid line indicated by the shoulder for the most intense band for specimen S1 before etching decomposed into two dashed lines of Gaussian profiles. The parameters of Gaussian profiles are listed in Table I.

$$I = A_1 e^{-[(k-k_1)/\alpha_1]^2} + A_2 e^{-[(k-k_2)/\alpha_2]^2} + \mathrm{B} \quad , \qquad (1)$$

where A, α, and k are the amplitude, Gaussian radius, and band position, respectively. B is a constant. Subscripts 1 and 2 denote respectively the major profile and minor profile. Figure 3 shows an example of shoulder consisting of two Gaussian profiles for specimen S1 before etching. The values of A_1, A_2, α_1, α_2, k_1, k_2, and B for the five specimens with different etching times are calculated and listed in Table I. It is found that the band for the most intense band is independent of etching time and located at 517.1, 523.1, 520.6, 519.4, and 521.6 cm^{-1}, respectively. The band for the minor profile shifts toward the long wave number when the etching time is increased for all machining processes. The band position of minor profile becomes stable at 514.9, 519.5, 520.3, 518.7, and 520.9 cm^{-1} after the etching time is greater than 10, 3, 5, 1, and 10 min, for specimens S1, S2, S3, S4, and S5, respectively. Thus, the depth of subsurface damage for S1, S2, S3, S4, and S5 samples are calculated to be 3.6, 1.08, 1.8, 0.36, and 3.6 μm. This means that the grinding and polishing is the least effective damage process in this study.

According to the experimental results of Raman spectra, the damage induced by lapping is comparable to the damage ground by 1200 mesh. The microcracks were examined using an optical microscope. There are many microcracks in the subsurface layer of the lapped specimen. In the ground specimen, however, no microcracks were found. Raman spectroscopy is very sensitive to re-

TABLE I. The values of A_1, A_2, α_1, α_2, k_1, k_2, and B for specimens S1, S2, S3, S4, and S5 with different etching times, t.

Specimen	t (min)	A_1	A_2	α_1 (cm^{-1})	α_2 (cm^{-1})	k_1 (cm^{-1})	k_2 (cm^{-1})	B
S1	0	4108	2072	11.46	55.90	515.7	473.8	537.1
	1	3368	445	7.95	54.23	517.2	489.5	107.8
	3	3376	410	8.39	27.02	516.9	514.9	105.2
	5	4193	447	6.33	22.30	516.4	514.5	69.0
	10	4159	440	6.38	22.47	517.1	514.9	74.0
S2	0	2079	531	12.14	51.99	522.8	495.0	220.4
	1	2294	406	12.70	51.99	521.0	495.6	227.5
	3	2605	483	11.64	29.36	523.3	519.5	175.3
	5	2599	488	11.56	29.11	523.1	519.5	172.6
S3	0	2663	566	10.90	57.73	520.8	491.1	209.5
	1	1490	409	13.93	55.05	521.0	491.7	191.7
	3	1109	427	11.49	25.48	521.0	519.4	192.1
	5	1636	823	11.06	25.73	520.6	520.3	168.4
S4	0	4937	649	8.93	29.11	519.7	518.5	89.6
	1	1811	327	9.62	28.63	519.1	518.7	324.4
	3	2483	231	9.17	30.29	519.4	518.7	80.9
S5	0	2063	303	13.04	33.33	522.0	523.1	192.1
	5	2058	543	10.23	28.63	521.7	519.8	101.7
	10	1862	208	13.36	33.52	522.0	518.8	98.3
	30	1989	195	12.91	39.53	521.6	520.9	91.8

sidual stresses rather than to microcracks. The damage in the lapped specimen is more severe than that in the ground specimen.

TEM examination was conducted to find defects in the damaged layers. Figure 4 shows the cross-sectional TEM micrograph for specimen S1, indicating dislocations and stacking faults. However, dislocations were not found in the cross-sectional TEM micrograph. The quantitative relation between defects and Raman spectroscopy will be investigated in the future. The distance from defect to surface is estimated to be about 3.5 μm in Fig. 3 and 0.30 μm in Fig. 4. The result is consistent with the micro-Raman analysis.

This work studies subsurface damage in machined silicon wafers using micro-Raman spectroscopy that was incorporated with wetting etching. The silicon wafers under different machining processes of grinding (1200, 4000, and 8000 mesh, grinding and polishing, and lapping) are assigned as S1, S2, S3, S4, and S5, respectively. The machined specimens were etched in 40% KOH solution for different periods. Both the shape and intensity for the shoulder (450–570 cm^{-1}) of the most intense band and the second band (300 cm^{-1}) regions are changed for the machined wafers. Both shoulder and second band intensities decrease with increasing etching depth until the damage layer was etched out. The shoulder for the most intense band can be fitted using the sum of two Gaussian profiles. The band for the major profile is always located at 514.7, 519.5, 519.9, 519.2, and 520.7 cm^{-1} for specimens S1, S2, S3, S4, and S5, respectively. The band position for the minor profile shifts toward the long wave number as the etching time is increased until it reaches a stable value. The above results show that the depth of damage layer is 3.6, 1.08, 1.8, 0.36, and 3.6 μm for specimens S1, S2, S3, S4, and S5, respectively.

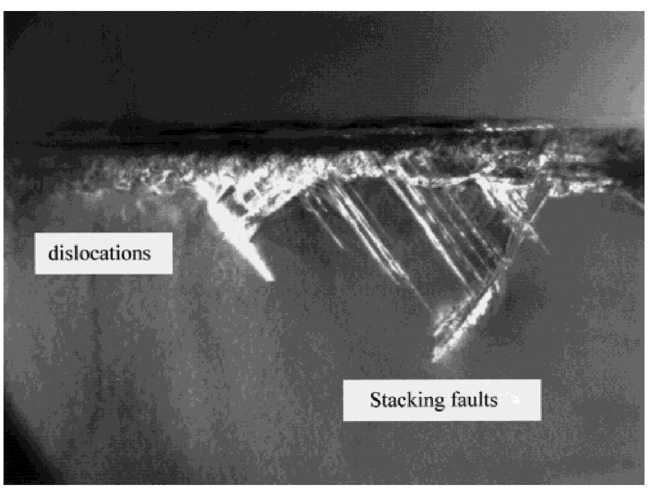

FIG. 4. Cross-sectional TEM micrograph for specimen S1 (13,600×). There are many dislocations and (111) stacking faults at the subsurface damage layer.

The micro-Raman spectrum can be applied to measure the depth of damage layer. Direct evidence of damage layer is provided by the microstructure. According to TEM results, dislocations and stacking faults are responsible to this damage layer. However, many microcracks appear in lapped specimens and not in the ground specimens.

ACKNOWLEDGMENTS

The work of L-Q.C., X.Z., and T-Y.Z. was supported by the Hong Kong Research Grants Council, and the work of S.L. was supported by the National Science Council of Taiwan.

REFERENCES

1. J.F. Scott and B. Pouligny, J. Appl. Phys. **64,** 1547 (1988).
2. C.A.P. Dearaujo, L.D. McMillan, B.M. Melnik, J.D. Cuchiaro, and J.F. Scott, Ferroelectrics **104,** 241 (1990).
3. P.A. McKeown, Ann. CIRP **36,** 495 (1987).
4. N. Taniguchi, Ann. CIRP **32,** 573 (1983).
5. U. Bismayer, E. Brinksmerier, B. Güttler, H. Seibt, and C. Menz, Precis. Eng. **16,** 139 (1994).
6. H. Hashimoto, H. Itoh, H. Eda, and K. Kishi, Proc. Int. Conf. Prod. Eng. **5,** 603 (1984).
7. M. Cardona, Proc. SPIE **822,** 2 (1987).
8. R.G. Sparks and M.A. Paesler, J. Appl. Phys. **71,** 891 (1992).
9. J. Verhey, U. Bismayer, B. Güttler, and H. Lundt, Semicond. Sci. Technol. **9,** 404 (1994).
10. E. Brinksmeier, Precis. Eng. **11,** 211 (1989).
11. S. Johansson and J.A. Schweitz, J. Am. Ceram. Soc. **71,** 617 (1988).
12. R.G. Sparks and M.A. Paesler, Precis. Eng. **10,** 191 (1988).
13. H.K. Tonshoff, W.V. Schmieden, I. Inasaki, W. Konig, and G. Spur, Ann. CIRP **39,** 621 (1990).
14. R.J. Nemanich, in *Materials Characterization,* edited by N.W. Cheung and M-A. Nicolet (Mater. Res. Soc. Symp. Proc. **69,** Pittsburgh, PA, 1986), p. 23.
15. G. Contreras, A.K. Sood, M. Cardona, and A. Campaan, Solid State Commun. **49,** 303 (1984).
16. P.M. Fauchet and I.H. Campbell, CRC Crit. Rev. Solid State Mater. Sci. **14,** S79 (1988).
17. E. Anastrassakis, A. Pinezuk, E. Burstein, F.H. Pollak, and M. Cardona, Solid State Commun. **8,** 133 (1970).
18. F. Cerdeira, C. Buchenauer, F. Pollak, and M. Cardona, Phys. Rev. B **5,** 580 (1972).